Journal of Molecular Catalysis A: Chemical 315 (2010) 205–212

Contents lists available at ScienceDirect

Journal of Molecular Catalysis A: Chemical

journal homepage: www.elsevier.com/locate/molcata

Preparation and characterization of Mesopoous VO_x/SBA-16 and their application for the direct catalytic hydroxylation of benzene to phenol

Yujun Zhu[a,*], Yongli Dong[a,b], Lina Zhao[a], Fulong Yuan[a,*]

[a] Key Laboratory of Functional Inorganic Material Chemistry, Ministry of Education, School of Chemistry and Materials, Heilongjiang University, Harbin, 150080, PR China
[b] Analysis and Testing Center, Heilongjiang Institute of Science and Technology, Harbin, 150027, PR China

ARTICLE INFO

Article history:
Received 30 June 2009
Received in revised form
20 September 2009
Accepted 21 September 2009
Available online 27 September 2009

Keywords:
Vanadium
SBA-16
Benzene
Hydroxylation

ABSTRACT

Vanadium oxide supported on mesoporous SBA-16 (VO_x/SBA-16) catalysts have been prepared by the impregnation method and characterized by small-angle XRD, wide-angle XRD, TEM, N_2-physisorption, DRUV–vis, Raman spectrum and H_2-TPR. The VO_x/SBA-16 catalysts retained the cubic cage-like pore structure of SBA-16. The dispersion and the nature of the vanadium species depend strongly on the V amount. At V loading of less than 3.6 wt%, isolated tetrahedral VO_4 is the main existence species that is highly dispersed in the pores of the support SBA-16. With the increase in V loading, the aggregation of isolated tetrahedral VO_4 species occurred to form polymerized VO_4 units. When the V loading was above 5.5 wt%, nanostructured V_2O_5 crystallites were formed besides aggregation of polymerized VO_4 units. VO_x/SBA-16 with 7.3 wt% V showed excellent activity for the hydroxylation of benzene. The effect of reaction time, temperature and the amount of catalyst was investigated over VO_x/SBA-16 (7.3 wt%) catalyst. The highest phenol yield and turnover number were 13.8% and 32.4, respectively, which were attributed to the formation of highly dispersed VO_4 species and polymerized VO_4 units. The TON and yield of phenol also increase in the presence of the V_2O_5 crystallites but its selectivity decreases.

1. Introduction

Phenol is an important chemical material, which is the major source of phenol resins, fibers, caprolactam, adipic acid, dyestuffs and medicine [1,2]. The worldwide production of phenol is mostly obtained by a well-known three-step process called the cumene process, which produces acetone as a byproduct in equimolar amount and restricts the industrial production of phenol [3]. Accordingly, the direct hydroxylation of benzene to phenol has attracted much attention in terms of an environment-friendly green process and economic efficiency. Studies on direct oxidation of benzene to phenol with various oxidants, such as nitrous oxide [4,5], hydrogen peroxide [6–9], molecular oxygen [10,11] or a mixture of oxygen and hydrogen [12] have been reported. The direct hydroxylation of benzene with hydrogen peroxide as oxidant is widely attempted as a green process at the mild conditions [7–9,13], which would be one of the most useful processes in the future [14]. However, it is a challenge to the higher yield and selectivity of phenol in the process of hydroxylation of benzene, since phenol is more reactive toward oxidation than benzene itself, substantial formation of over-oxygenated byproducts (benzoquinone, catechol, hydroquinone and tars) also occurs [15].

Compounds of vanadium, due to their highly feasible reactivity and remarkable stability, have been utilized as efficient catalysts for a variety of oxidation reactions, especially for the hydroxylation of alkanes and aromatic compounds [15–26]. There were several reports about the benzene to phenol reaction over vanadium-containing catalysts, such as VO_x species anchored on amorphous siliceous microporous mixed oxides and MCM catalysts [15,16], VO_x species supported on SBA-15 [10] and clay [18], vanadium-substituted polyoxometalates [19–23] and phosphomolybdates [24] and sodium metavanadate [25]. Lemke et al. have used vanadium supported on mesoporous siliceous structures of MCM-type, silica of Aerosol® 300-type and amorphous siliceous microporous mixed oxides as catalysts for the direct oxidation of benzene to phenol. Best results of hydroxylation of benzene were obtained on a low vanadium-containing VO_x/SiO_2 catalyst. However, the selectivity of phenol was below 60% when the conversion of benzene was higher than 10% [15]. Lee et al. reported catalytic hydroxylation of benzene over vanadium-containing molecular sieves (MCM-41, MCM-48, BEA and MFI). V-MCM-41 showed the highest activity where the selectivity of phenol was 93%, but the conversion of benzene was only 1.39% [26]. Vanadium-substituted polyoxometalates (polyoxomolybdates [20–22], polyoxotungstates [23]) and phosphomolybdates [24] catalysts on benzene hydroxyla-

* Corresponding authors. Tel.: +86 451 86608610; fax: +86 451 86673647.
E-mail addresses: yujunzhu@hlju.edu.cn, yujunzhu@126.com (Y. Zhu), fulongyuan2000@yahoo.com (F. Yuan).

1381-1169/$ – see front matter © 2009 Elsevier B.V. All rights reserved.
doi:10.1016/j.molcata.2009.09.013

tion with hydrogen peroxide have been well investigated. These catalysts showed a high stability and gave a steady performance by being reused in oxidation recycle in which the phenol yield was up to 10% with phenol selectivity about 85%. However, from the synthetic viewpoint, selectivity site-substituted vanadium (V) polyoxometalates have been very difficult to prepare.

Previous studies have shown that the catalytic performance of supported vanadia catalysts crucially depends on the structure and distribution of the surface vanadium oxide species [16,26–32]. To a certain extent, the effect of the different supports on the dispersed surface vanadium oxide species is important. Mesoporous materials as catalyst support has been attracted much attention since the development of the M41S family [33,34] because of their large surface area, uniform pore size, big pore volume and well-ordered structure. In the family of mesoporous materials, SBA-15 and SBA-16 materials exhibit thicker pore walls and higher hydrothermal stability than M41S [35]. In particular, SBA-16 which has three-dimensional channel and cubic (*Im3m*) cage structured mesoporous silica structure [36,37] can be more favorable for mass transfer kinetics than the unidirectional pore system of other hexagonal mesoporous phases. Studies of vanadium supported on SBA-15 have been extensively reported for applications in the literature [10,29,38–40]. However, relatively few papers have been published on SBA-16 as support [41]. Recently, researchers have paid more attention to SBA-16 and its application in catalysis based on its structure character [42–47].

In this paper, a series of VO_x/SBA-16 catalysts were prepared by impregnation method for the first time, and their catalytic performance was tested for the benzene hydroxylation. The vanadium species and its dispersion on the surface of VO_x/SBA-16 catalysts were discussed. The relationship between vanadium species and catalytic activity was also investigated.

2. Experimental

2.1. Catalyst preparation

2.1.1. SBA-16 support synthesis

The SBA-16 silica was prepared under acidic condition, using Pluronic F127 as a structure-directing agent and TEOS as the silica source [35]. The molar composition of the reaction mixture was 1 TEOS: 7.14×10^{-3} F127: 3×10^{-2} HCl: 2.8 H_2O: 21.74-43.48 EtOH, and the homogeneous solution was stirred vigorously for 1 h at 70 °C. After ageing overnight at 50 °C, the product was dried in air at 80 °C. Finally, the product was calcined under ambient atmosphere at 550 °C with a heating rate of 1 °C min^{-1} and an isothermal period of 4 h.

2.1.2. VO_x/SBA-16 by impregnation

VO_x/SBA-16 catalysts with different V loading were prepared as follows: an amount of aqueous solution of NH_4VO_3 (0.010 molL^{-1}) at the appropriate contents was placed in vessel of a vacuum rotary evaporator [15]. 1 g of support SBA-16 was added, and the slurry was briefly evacuated to remove residual air from the pores. Afterwards, water was evaporated at 55 °C. The solid was dried at 80 °C for 12 h and calcined at 400 °C with a heating rate of 1 °C min^{-1} in air for 4 h, a light yellow powder was obtained.

2.2. Catalyst characterization

Small-angle X-ray diffraction (SAXRD) measurements were carried out on a Rigaku D/Max-2400X X-ray diffractometer Cu Kα (λ = 1.5406 Å) radiation (40 kV and 200 mA).

Wide-angle X-ray diffraction measurements (WAXRD) were performed on a Rigaku D/Max-IIIB Cu Kα (λ = 1.5406 Å) radiation (40 kV and 20 mA) and Ni filter. The patterns were collected from $10 < 2\theta < 60$.

The nitrogen physisorption experiments were performed at −196 °C on a Quantachrome Autosorb-1 automated gas adsorption system. The sample was outgassed at 300 °C for 4 h before the measurement. The pore size distribution was calculated from the desorption branch of the isotherm using the BJH method.

Transmission electron microscopy (TEM) measurements were taken on a FEI Tecnai G2 S-Twin electron microscope operating at 200 kV. High resolution transmission electron microscopy (HRTEM) measurements were carried out using a FEI Tecnai F30 electron microscope operating at 300 kV.

The diffuse reflectance ultraviolet–visible (DRUV–vis) spectroscopy were recorded on a Shimadzu UV-2550 spectrophotometer equipped with an integrating sphere attachment (ISR-2200). $BaSO_4$ was the reference material. The sample was heated at 300 °C for 0.5 h before test.

The Raman spectrum studies were carried out using a HR800 (JY) spectrometer with a Ar^+ ion laser (458 nm). The laser was operated at a power level of 20 mW measured at the sample using a power meter (Coherent).

Temperature-programmed reduction with hydrogen (H_2-TPR) of the catalysts was measured in a conventional self-made apparatus equipped with thermal conductivity detector (TCD). 30 mg of the catalyst (40–60 mesh) was mounted in a quartz tube and calcined in He flow (20 mL min^{-1}) at 300 °C for 1 h with the aim to remove the physisorbed substances while 10 mg V_2O_5 was used as a comparison test. The sample was reduced with a 5% H_2/N_2 mixture (20 cm^3 min^{-1}) by being heated to 650 °C at a rate of 10 °C min^{-1}.

2.3. Catalytic evaluation

Hydroxylation of benzene with 30% aq. H_2O_2 was run in a 30 mL double layer glass reactor equipped with a reflux condenser, a magnetic stirrer and a superthermostat. The standard condition was as follows: 6.0–20 mg of catalyst, 0.30 mL (3.36 mmol) of benzene and 5 mL of CH_3CN were added. After the mixture was heated to the desired temperature (50–70 °C), 0.8–1.5 mL (7.83–17.62 mmol) of 30% aq. H_2O_2 was added, and reaction was carried out under these conditions for 1–8 h.

The liquid products were analyzed by gas chromatograph (SP-2100 China, FID detector) with an OV-1 capillary column (30 m × 0.25 mm × 0.33 μm). Phenol, benzoquinone, catechol, and hydroquinone in the products were further identified by GC–MS (Agilent 6890/5973N). The quantitative analysis of the mixture was determined by the calibration curves, using toluene as the internal standard.

3. Results and discussion

3.1. Pore structure of catalysts

Fig. 1 shows the small-angle X-ray diffraction (SAXRD) patterns of VO_x/SBA-16 catalysts with different amounts of V loading. All the patterns were similar to each other and showed a very strong (1 1 0) reflection (0.97° 2θ) of the cubic (*Im3m*) structure with a lattice constant of a_0 = 12.8 nm [42], which indicated that the uniform pore structure of SBA-16 was well retained and the vanadium species may be highly dispersed on the surface of SBA-16 mesoporous silicas. In addition, it is obviously observed that the patterns of VO_x/SBA-16 composites showed a decrease in peak intensity with increasing vanadia loading. This is probably due to the difference on the scattering contrasts of the pores and the walls and the formation of nanostructured VO_x species inside the pores of SBA-16 [48,49]. For these SBA-16 samples (2 0 0) and (2 1 1) reflections,

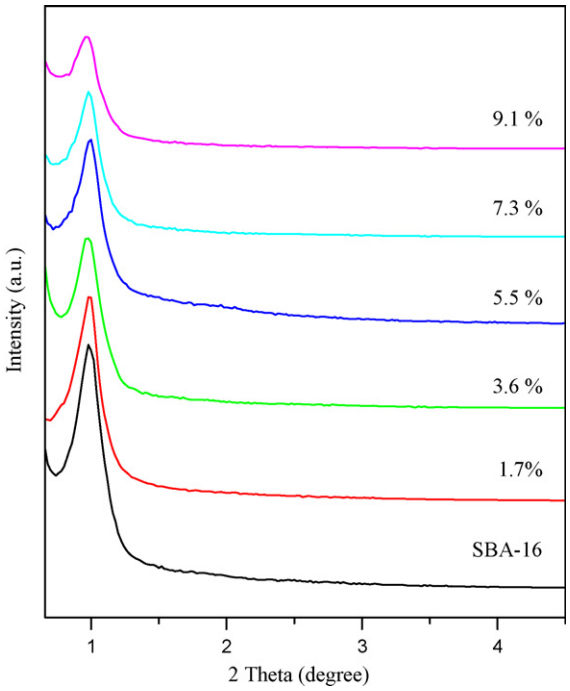

Fig. 1. SAXRD patterns of VO_x/SBA-16 catalysts.

which were also characteristic of a cubic cage-like (*Im3m*) structure, were not clearly observed in the SAXRD patterns (Fig. 1) as reference described [35]. Further evidence for the cubic meso-structure was provided by the TEM images in Fig. 2.

The TEM images (Fig. 2) of the support SBA-16 molecular sieves and VO_x/SBA-16 catalysts show that they all have well-ordered cubic mesoporous along the (1 0 0) and (1 1 1) directions, and the pore opening was about 40 Å in diameter. These results confirm that the support SBA-16 has a 3-D cubic pore structure (*Im3m*) [36,37,50], and its structure can remain consistent after the impregnation by vanadia species. So SBA-16 offers a good matrix to support highly dispersed V species.

The N_2-physisorption isotherms and pore size distribution for all the VO_x/SBA-16 catalysts and SBA-16 are shown in Fig. 3. It is clear that the N_2-physisorption isotherm of SBA-16 is the type IV with a typical H_2 hysteresis loop and a narrow pore size distribution, which indicate that they have the characteristic of cage-like (*Im3m*) pore structure of SBA-16. After the impregnation, the isotherms of VO_x/SBA-16 catalysts retained their shape, which could be an indication for maintenance of the mesoscopic order of the parent materials [41]. The data of surface area and pore volume are shown in Table 1. With the increase in the amount of V loading from 0 to 9.1 wt%, the surface area of the catalyst decreased from 382.0 to 194.4 m^2g^{-1}, accompanied with the decease in the pore volume, which suggested that the vanadia species was located mainly inside the pores, coating the inner walls of the SBA-16 mesoporous silica matrix [28]. It is also interesting to stress on the negligible change in its pore diameter observed for VO_x/SBA-16 with larger decrease in the pore volume and BET surface area. The reason may be that partial pores

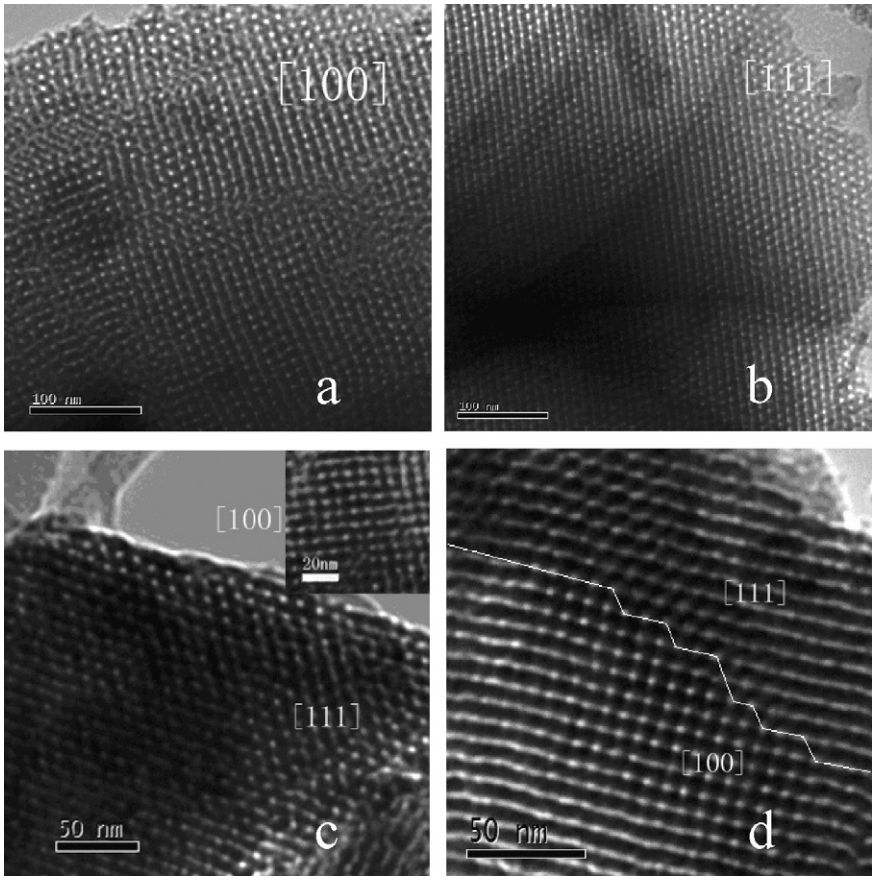

Fig. 2. TEM images of the support mesoporous SBA-16 along [1 0 0] direction (a), [1 1 1] direction (b) and VO_x/SBA-16 with 3.6 wt% of V loading (c), 7.3 wt% of V loading (d).

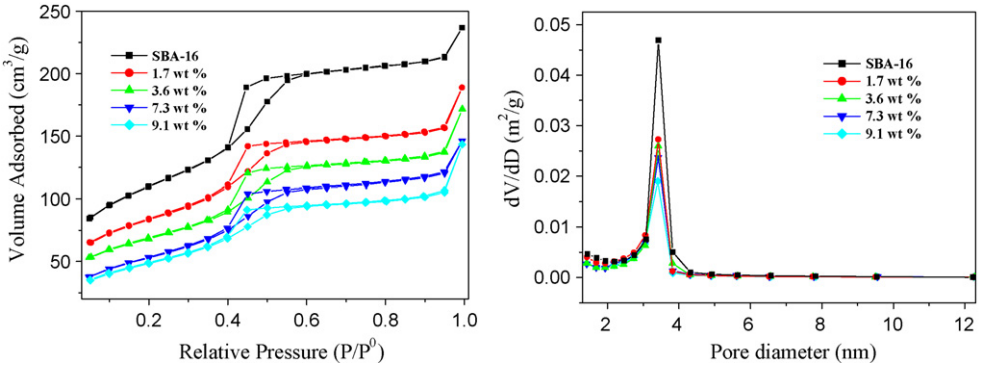

Fig. 3. N_2-physisorption isotherm and pore size distribution of VO_x/SBA-16 catalysts.

Table 1
Texture properties of SBA-16 and VO_x/SBA-16 catalysts.

Sample	S_{BET}[a] ($m^2\ g^{-1}$)	V_{total}[b] ($cm^3\ g^{-1}$)	D_{BJH}[c] (Å)
SBA-16	382.0	0.367	34.23
1.7 wt% VO_x/SBA-16	273.1	0.285	34.22
3.6 wt% VO_x/SBA-16	222.9	0.258	34.21
7.3 wt% VO_x/SBA-16	217.4	0.239	34.17
9.1 wt% VO_x/SBA-16	194.4	0.230	34.07

[a] BET specific surface area.
[b] Total pore volume.
[c] Diameter of the pore.

were blocked by the VO_x species as Tsoncheva et al. described [41].

From the X-ray diffraction, TEM images and N_2-physisorption isotherm discussed above, it clearly that all of the VO_x/SBA-16 samples retained the ordered cubic cage-like (*Im3m*) pore structure of SBA-16. Thus, the introduced vanadium species may be highly dispersed on the surface of SBA-16 mesoporous silicas.

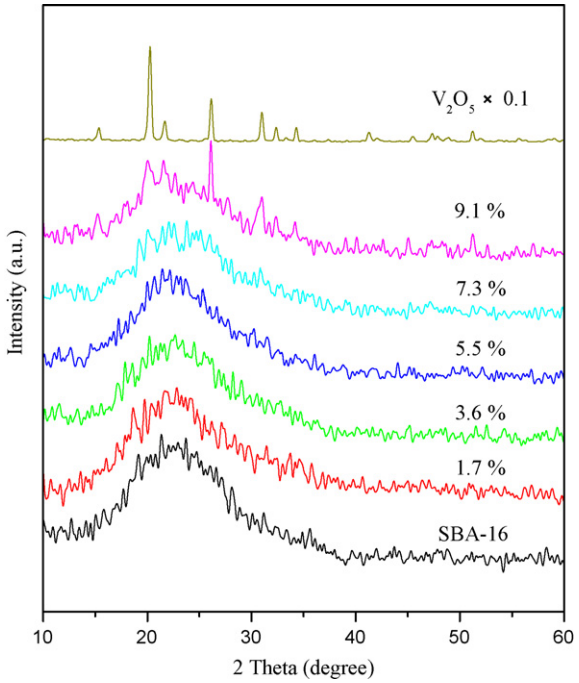

Fig. 4. WAXRD patterns of VO_x/SBA-16 catalysts.

3.2. Study of V species

3.2.1. Wide-angle XRD

The WAXRD patterns of VO_x/SBA-16 catalysts with different amounts of V loading are shown in Fig. 4. When V loading was from 1.7 to 7.3 wt%, a similar profile like amorphous SiO_2 of the parent SBA-16 was presented and no characteristic reflections of V_2O_5 phase were observed, which may be due to formation of the high dispersed V species on the surface of SBA-16 that was not identified by XRD method. At higher V loading (9.1 wt%), V_2O_5 phase (2θ = 20.1, 21.5, 26.1 and 31.0° *PDF 077-2418*) was observed, which revealed a decrease in V dispersion on the surface of SBA-16. In combination with the patterns of SAXRD (Fig. 1), a significant decrease in peak intensity, which could be an indication of decrease in the regularity of the pore structure, was caused by the formation of bulk V_2O_5 with the decrease in V dispersion.

3.2.2. H_2-TPR

Fig. 5 shows the H_2-TPR curves of VO_x/SBA-16 catalysts with different amounts of V loading. A comparative profile of the bulky V_2O_5 sample obtained from NH_4VO_3 by calcination is also presented. In Fig. 5, we can see that all the H_2-TPR profiles of VO_x/SBA-16 catalysts exhibited a major reduction peak at temperature range between 550 and 600 °C. And the curves of VO_x/SBA-16 samples showed a second reduction peak at around 650–700 °C when V loading was up to 7.3 wt%. According to the literature [16], low-temperature reduction stage was ascribed to the presence of highly dispersion of VO_x species, which could be located mainly

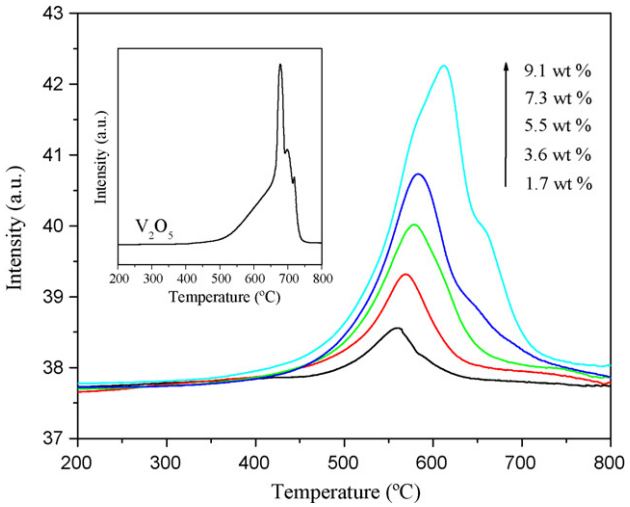

Fig. 5. H_2-TPR profiles of VO_x/SBA-16 catalysts.

Table 2
Data of H_2-TPR measurement of VO_x/SBA-16 catalysts.

Catalysts	LT-peak[a] (°C)	HT-peak[b] (°C)	$R_{LT\text{-}peak}$[c] (%)	$R_{HT\text{-}peak}$[d] (%)
1.7 wt% VO_x/SBA-16	560	–	100	0
3.6 wt% VO_x/SBA-16	569	–	100	0
5.5 wt% VO_x/SBA-16	579	–	100	0
7.3 wt% VO_x/SBA-16	584	650	97.4	2.6
9.1 wt% VO_x/SBA-16	610	658	93.5	6.5

[a] The temperature of low-temperature reduction peak.
[b] The temperature of high-temperature reduction peak.
[c] Ratio of LT-Peak area to the whole peak area.
[d] Ratio of HT-Peak area to the whole peak area.

inside the pores of parent SBA-16 [40]. Compared with the reduction peak of bulk V_2O_5 at around 678 °C, the high-temperature reduction peak can be attributed to reduction in the crystal V_2O_5 species on the surface of SBA-16 [51].

With the V loading increasing from 1.7 to 9.1 wt%, the low-temperature reduction peak shifted to the higher temperature value given in Table 2, which may be due to the formation of bigger particle size of aggregated VO_x species [34]. The ratio of the high-temperature reduction peak area to the whole peak area increases from 2.6% to 6.5% with the increase in the amount of V loading from 7.3 to 9.1 wt% (Table 2), which indicates that the amount of bulky V_2O_5 species increases with the amount of V loading. And these assignments will be further discussed by the following characterizations of DRUV–vis and Raman spectra.

3.2.3. Raman spectra

The supported vanadium oxide catalysts can be present in several VO_x structures such as isolated tetrahedral VO_4 species, polymeric species and crystalline V_2O_5 [28]. Here, laser Raman spectrum was used to elucidate the structure of vanadia species supported on SBA-16. Fig. 6 depicts the Raman spectra of VO_x/SBA-16 catalysts. At lower amount of V loading (<3.6 wt%), the spectrum was dominated by a strong band at around 1035 cm^{-1} with a small shoulder band at 1068 cm^{-1}, which was characteristic for the V=O stretch vibration of isolated tetrahedral VO_4 species (Td-V^{5+}) [28,32]. When the V loading got to 5.5 wt%, the spectrum shows an obvious difference from that of below 5.5 wt%. The intensity of the band assigned to tetrahedral VO_4 decreased, which indicated that the aggregation of isolated tetrahedral VO_4 species occurred to form polymerized VO_4 units. Moreover, it is noticed that an additional band at 998 cm^{-1} attributed to crystallite V_2O_5 appeared [28,32]. However, the highly dispersed vanadium species is still dominating. The band at 1035 cm^{-1} became broader and the intensity of the band at 998 cm^{-1} increased when the amount of V loading was up to 7.3 wt%, which showed more polymerized VO_4 units and crystalline V_2O_5 were obtained. These results reveal that an aggregation of partial V occurred on the surface of the VO_x/SBA-16 catalysts with increasing V loading. And the aggregation of V may not only lead to the formation of nanostructured polymerized VO_4 units, but also result in the formation of nanostructured V_2O_5 crystallites. The crystalline V_2O_5 species is minute on the surface of VO_x/SBA-16 (7.3 wt%) catalyst that can easily be measured by Raman but not be detected by XRD or H_2-TPR [27,32].

However, at the higher amount of V loading (9.1 wt%), the band at 998 cm^{-1} became a small shoulder peak and its intensity decreased. Simultaneously, a band at around 1022 cm^{-1} appeared and dominated the spectrum, which was assigned to hydrated surface vanadium oxide species forming a $V_2O_5 \cdot nH_2O$ on the VO_x/SBA-16 sample [27].

3.2.4. DRUV–vis spectra

The DRUV–vis spectra were recorded in order to understand the nature of observed coordination of V^{5+} ions in the VO_x/SBA-16. As shown in Fig. 7, all the spectra of VO_x/SBA-16 samples displayed a band at about 220 nm which was assigned to the silica materials [17,26]. At lower V loading, the profile of VO_x/SBA-16 (1.7 wt%) exhibited one strong absorption band at around 262 nm with two very weak shoulders at 303 and 405 nm, which could be ascribed to the charge-transfer transitions of the ligand O^{2-} to metal center V^{5+} for the isolated tetrahedral VO_4 species ($O_{3/2}V{=}O$), polymerized tetrahedral VO_4 species and square pyramidal V^{5+}, respectively [28]. The appearance of square pyramidal V^{5+} species may be caused by the coordination of H_2O and tetrahedral VO_4 species. However, the square pyramidal V^{5+} species have not been detected in Raman spectra (Fig. 6). The reason is that the H_2O molecule would be departed from the square pyramidal V^{5+} species by the irradiation of intensive laser in Raman testing. With the increase in the

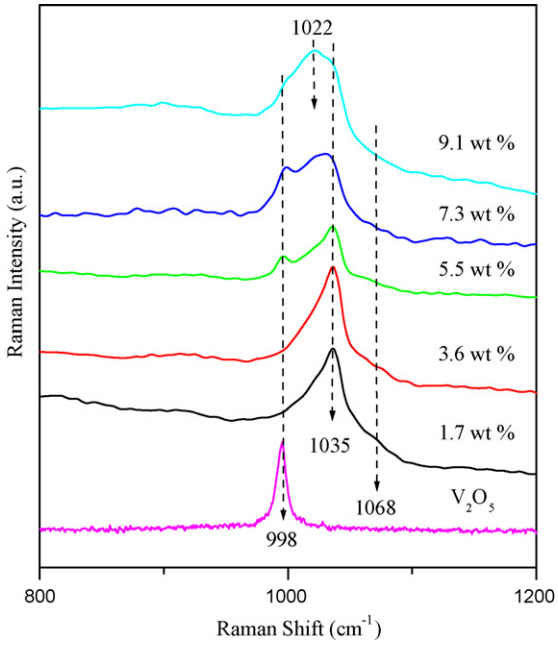

Fig. 6. Raman spectrums of VO_x/SBA-16 catalysts.

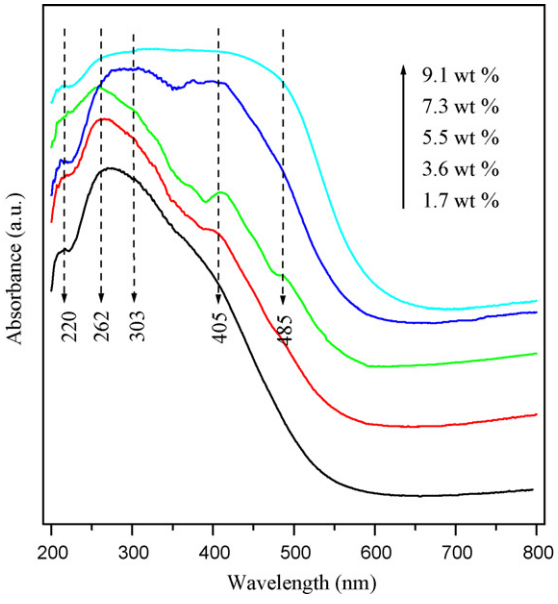

Fig. 7. DRUV–vis spectra of VO_x/SBA-16 catalysts.

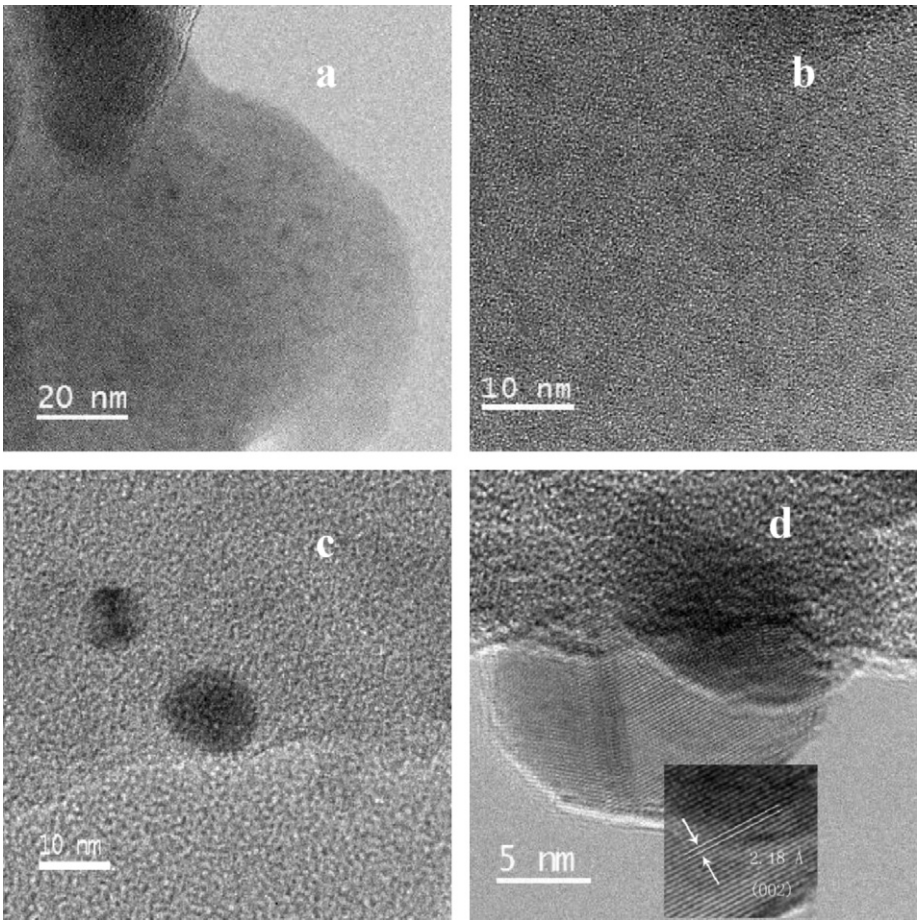

Fig. 8. HRTEM images of 3.6 wt% VO_x/SBA-16 (a and b) and 7.3 wt% VO_x/SBA-16 (c and d).

amount of V loading, both the bands at 303 and 405 nm shifted to higher wavelength slightly, and their intensities increased. When the amount of loading was up to 5.5 wt%, one additional absorption band at around 485 nm was observed which could be associated with the presence of octahedral V^{5+} species, as above-mentioned V_2O_5 crystallites that have been detected by Raman spectra. The absorption bands changed significantly when the amount of V loading reached 7.3 wt%. The intensities of all the absorption bands at around 303, 405 and 485 nm increased significantly. It can be concluded that some isolated V centers on the surface of catalyst aggregated and changed to be polymerized VO_x species with V loading. At the higher amount of V loading (9.1 wt%), the absorption band showed a noticeable red shift, and the maximum absorption signal began from about 485 nm. It can be attributed to the formation of bulk V_2O_5 on the VO_x/SBA-16. In a word, the types of vanadia species in these catalysts are strongly influenced by the V concentration [28].

These results are in agreement with the characterization of H_2-TPR and Raman spectra, which reveal an aggregation of V species on the surface of VO_x/SBA-16 catalysts with increasing the amount of V loading.

3.2.5. HRTEM

The HRTEM images of VO_x/SBA-16 catalysts are shown in Fig. 8. There were only highly dispersed vanadia species on the VO_x/SBA-16 (3.6 wt%) catalyst (Fig. 8a and b). However, some composites of polymerized VO_4 species (Fig. 8c) with a diameter size around 10 nm and some nanostructured microcrystal of V_2O_5 (Fig. 8d) outside the pores were observed for the VO_x/SBA-16 (7.3 wt%).

These results are in accordance with the analysis of Raman, DRUV–vis, H_2-TPR and XRD spectra, which demonstrate that the molecular structure of the surface vanadia species varies significantly with increasing the amount of V loading. In a word, the formation of high dispersed vanadia species is confirmed on the surface of SBA-16 when the amount of V loading is less than 5.5 wt%. On the surface of VO_x/SBA-16 (7.3 wt%) catalyst, the aggregation of the vanadium centers results in the formation of V_2O_5 crystallites besides the small VO_x clusters [32].

3.3. Catalytic tests

3.3.1. Hydroxylation of benzene with different V loading

The catalytic activities of VO_x/SBA-16 catalysts have been assessed in the liquid phase hydroxylation of benzene using H_2O_2 as oxidation. Fig. 9 depicts the influence of the amount of V loading on the catalysis activities. There was no activity for the parent SBA-16 in our experiment condition. However, phenol was obtained by benzene hydroxylation over the VO_x/SBA-16 catalysts prepared by the incorporation of vanadium on the surface of SBA-16. Benzoquinone was the primary byproduct for the present research. As was illustrated, the yield of phenol increased with V loading firstly, and obtained the maximum one when the amount of V loading was 7.3 wt%, and then decreased slightly with the further increase in the amount of V loading. The catalytic turnover number based on vanadium varied in a similar trend as the phenol yield. In comparison, the selectivity to phenol decreased slightly with increasing V loading, and it was always higher than 97.5% in each case. The highest phenol yield and turnover number (TON) over VO_x/SBA-16

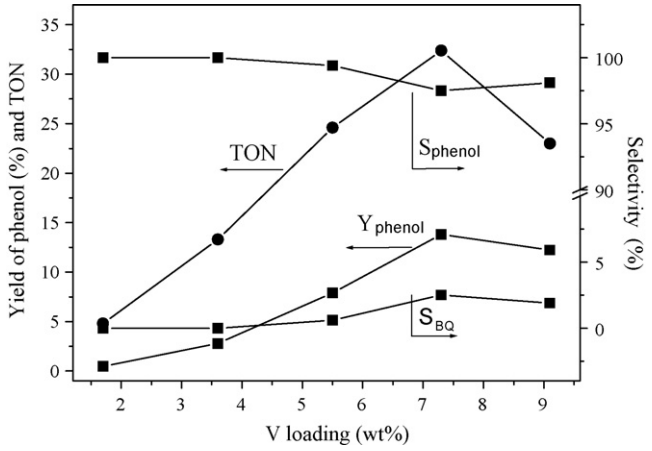

Fig. 9. Catalytic activity of benzene hydroxylation over VO_x/SBA-16 catalysts (reaction condition: 0.3 mL of benzene, 5 mL of acetonitrile and 1.5 mL of 30% aq. H_2O_2, 60 °C for 4 h, 0.010 g of catalyst weight).

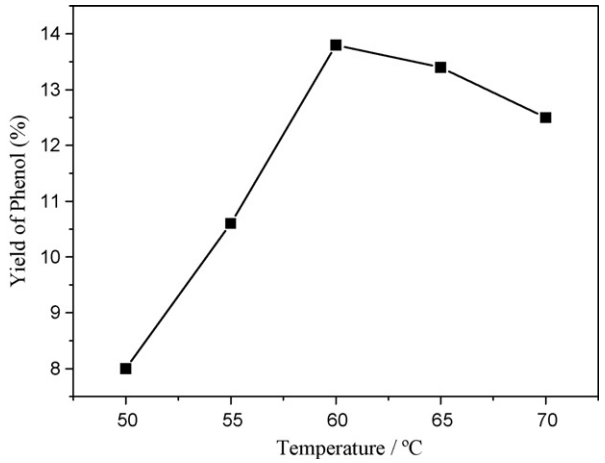

Fig. 10. Effect of different reaction temperature on yield of phenol over VO_x/SBA-16 (7.3 wt%) (reaction condition: 1.5 mL of 30% aq. H_2O_2, 0.010 g of catalyst weight, for 4 h).

(7.3 wt%) were 13.8% and 32.4 with the selectivity of 97.5%, respectively.

In combination with the results of catalysts characterization, it shows that the highly dispersed vanadium species is favorable for obtained high selectivity of phenol but related to low benzene conversion, which is agreed with the literatures described [15,52]. With the aggregation of isolated tetrahedral VO_4 species occurred to form polymerized VO_4 units, the selectivity of phenol decreases slightly. However, the TON and yield of phenol increase significantly. The microcrystal of V_2O_5 obtained by aggregation of VO_4 species to a greater extent leads to the decrease in selectivity of phenol, whereas the catalytic activity increases from the results of the TON and yield of phenol. It reveals that the presence of the microcrystal of V_2O_5 has not depressed the activity. But the activity decreases with the increase in the size of V_2O_5 crystallite. The presence of bulk V_2O_5 that can be detected by XRD is undesired for the hydroxylation of benzene. It is indicated that the presence of the microcrystal of V_2O_5 facilities for hydroxylation of benzene compared with bulk V_2O_5. Thus, the VO_x/SBA-16 (7.3 wt%) catalyst exhibits excellent catalytic performance for hydroxylation of benzene, which may be attributed to the formation of highly dispersed VO_4 species and polymerized VO_4 units. The TON and yield of phenol also increase in the presence of the V_2O_5 crystallites but its selectivity decreases. The results can be assigned to the three-dimensional pore system of SBA-16 which should be advantageous for mass transport [15].

3.3.2. *Effect of reaction conditions*

Here, the effects of the various reaction conditions including temperature, time and the amount of the catalyst on the yield of phenol were also investigated over VO_x/SBA-16 (7.3 wt%) catalyst based on its excellent catalytic performance for hydroxylation of benzene. The results are presented in Figs. 10–12.

The effect of the reaction temperature on the yield of phenol is shown in Fig. 10. It is indicated that only 8.0% yield of phenol was obtained at 50 °C, showing a slow reaction. When the reaction temperature rose to 60 °C, a sharp increase in the phenol yield (13.8%) was obtained. This indicated that higher temperatures were beneficial to the hydroxylation reaction. However, further increase in temperature caused a decrease in phenol yield because of the further oxidation of products and the decomposition of hydrogen peroxide. Thus, the temperature range of 50–65 °C is more suitable for the present hydroxylation reaction. This is in agreement with the literatures [25,41].

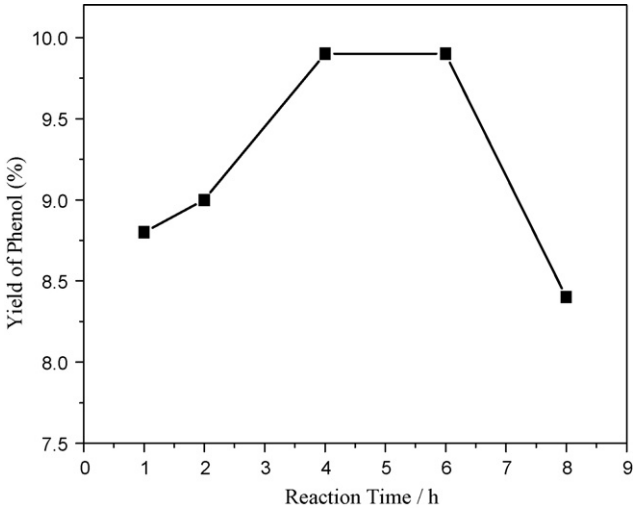

Fig. 11. Effect of different reaction time on yield of phenol over VO_x/SBA-16 (7.3 wt%) (reaction condition: 1.5 mL of 30% aq. H_2O_2, 60 °C, 0.010 g of catalyst weight).

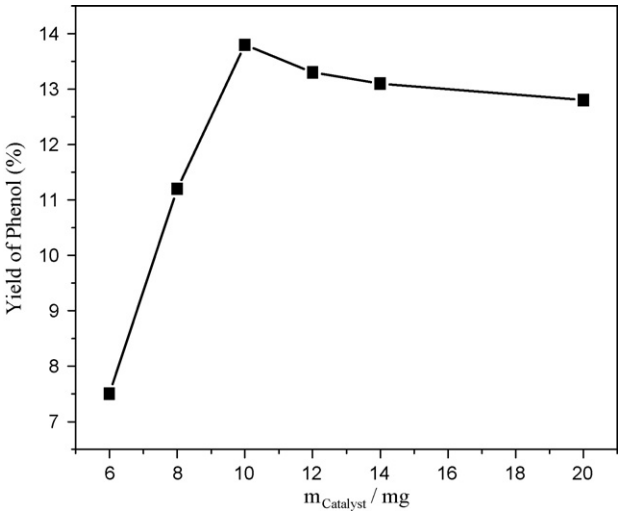

Fig. 12. Effect of the catalyst amount on yield of phenol over VO_x/SBA-16 (7.3 wt%) (reaction condition: 1.5 mL of 30% aq. H_2O_2, 60 °C for 4 h).

The effect of the reaction time on catalytic activity was investigated by several separate reactions under the same reaction conditions. Fig. 11 shows the yield of phenol as a function of reaction time. The amount of phenol formed quickly increased with time firstly, and it reached a plateau in the reaction period of 4–6 h. Then the yield of phenol decreased sharply, and here, the further oxidation of reaction products could occur.

Fig. 12 illustrates the influence of the amount of the catalyst between 6 and 20 mg. It can be seen that the yield of the phenol reached a higher value when the amount of the catalyst was 10 mg. The more the amount of catalyst used, the more catalytic active sites may be provided which are in favor of not only the hydroxylation of benzene but also the self-decomposition of hydrogen peroxide [18]. Thus, when the amount of the catalyst is over 10 mg, the phenol yield is not increase but slightly decrease due to the non-oxidative consumption of more hydrogen peroxide over excessive amount of catalyst.

4. Conclusion

SBA-16 supported vanadium oxide catalyst showed good catalytic performance for the direct hydroxylation of benzene to phenol by hydrogen peroxide under moderate condition. The satisfactory phenol yield and turnover number (TON) obtained with a selectivity of 97.5% over VO_x/SBA-16 (7.3 wt%) catalyst were 13.8% and 32.4 for 4 h, respectively. From the study of Raman spectra, DRUV–vis spectra, H_2-TPR and HRTEM, not only the highly dispersed VO_4 species, but also the polymerized VO_4 units and the microcrystal of V_2O_5 on the surface of catalyst may play a key role in the hydroxylation of benzene to phenol reaction.

Acknowledgements

This work is supported by the Natural Science Foundation of China (20876034), Major Foundation of Educational Commission of Heilongjiang Province of China (11531Z11) and Heilongjiang University Natural Science Funds for Distinguished Young Scholar (JCL200802).

References

[1] R.A. Sheldon, J.K. Kochi, Metal-Catalyzed Oxidations of Organic Compounds, Academic, New York, 1981, pp. 329–333.
[2] G. Goor, in: G. Strukul (Ed.), Catalytic Oxidations with Hydrogen Peroxide as Oxidant, Kluver, Dordrecht, 1992, pp. 29–31.
[3] L. Balducci, D. Bianchi, R. Bortolo, R. D'Aloisio, M. Ricci, R. Tassinari, R. Ungarelli, Angew. Chem. Int. Ed. 115 (2003) 5087–5090.
[4] I. Yuranov, D.A. Bulushev, A. Renken, L. Kiwi-Minsker, Appl. Catal. A: Gen. 319 (2007) 128–136.
[5] Y. Li, Z. Feng, R.A. vanSanten, E.J.M. Hensen, C. Li, J. Catal. 255 (2008) 190–196.
[6] J.K. Joseph, S. Singhal, S.L. Jain, R. Sivakumaran, B. Kumar, B. Sain, Catal. Today 141 (2009) 211–214.
[7] H.A. Xia, K.Q. Sun, K.J. Sun, Z.C. Feng, W.X. Li, C. Li, J. Phys. Chem. C 112 (2008) 9001–9005.
[8] V.S. Chemyavsky, L.V. Pirutko, A.K. Uriarte, A.S. Kharitonov, G.I. Panov, J. Catal. 245 (2007) 466.
[9] E.J.M. Hensen, Q. Zhu, R.A. van Santen, J. Catal. 233 (2005) 136–146.
[10] Y.Y. Gu, X.H. Zhao, G.R. Zhang, H.M. Ding, Y.K. Shan, Appl. Catal. A: Gen. 328 (2007) 150–155.
[11] T. Miyahara, H. Kanzaki, R. Hamada, S. Kuroiwa, S. Nishiyama, S. Tsuruya, J. Mol. Catal. A Chem. 176 (2001) 141–150.
[12] S. Niwa, M. Eswaramoorthy, J. Nair, A. Raj, N. Itoh, H. Shoji, T. Namba, F. Mizukami, Science 295 (2002) 105–107.
[13] D. Arntz, Catal. Today 18 (1993) 173–198.
[14] M.G. Clerici, in: R.A. Sheldon, H.V. Bekkum (Eds.), Fine Chemicals through Heterogeneous Catalysis, Wiley-VCH, Weinheim, 2001, pp. 538–549.
[15] K. Lemke, H. Ehrich, U. Lohse, H. Berndt, K. Jähnisch, Appl. Catal. A: Gen. 243 (2003) 41–51.
[16] L.D. Nguyen, S. Loridant, H. Launay, A. Pigamo, J.L. Dubois, J.M.M. Millet, J. Catal. 237 (2006) 38–48.
[17] C.H. Lee, T.S. Lin, C.Y. Mou, J. Phys. Chem. B 107 (2003) 2543–2551.
[18] X.H. Gao, J. Xu, Appl. Clay Sci. 33 (2006) 1–6.
[19] T. Sakamoto, T. Takagaki, A. Sakakura, Y. Obora, S. Sakaguchi, Y. Ishii, J. Mol. Catal. A: Chem. 288 (2008) 19–22.
[20] J. Zhang, Y. Tang, G. Li, C. Hu, Appl. Catal. A: Gen. 278 (2005) 251–261.
[21] K. Nomiya, Y. Nemoto, T. Hasegawa, S. Matsuoka, J. Mol. Catal. A: Chem. 152 (2000) 55–68.
[22] K. Nomiya, S. Matsuoka, T. Hasegawa, Y. Nemoto, J. Mol. Catal. A: Chem. 156 (2000) 143–152.
[23] K. Nomiya, H. Yanagibayashi, C. Nozaki, K. Kondoh, E. Hiramatsu, Y. Shimizu, J. Mol. Catal. A: Chem. 114 (1996) 181–190.
[24] J. Chen, S. Gao, J. Xu, Catal. Commun. 9 (2008) 728–733.
[25] M. Jian, L.F. Zhu, J.Y. Wang, J. Zhang, G.Y. Li, C.W. Hu, J. Mol. Catal. A: Chem. 253 (2006) 1–7.
[26] C.W. Lee, W.J. Lee, Y.K. Park, S.-E. Park, Catal. Today 61 (2000) 137–141.
[27] C. Hess, J. Catal. 248 (2007) 120–123.
[28] C. Hess, J.D. Hoefelmeyer, T. Don Tilley, J. Phys. Chem. B 108 (2004) 9703–9709.
[29] G. Du, S. Lim, M. Pinault, C. Wang, F. Fang, L. Pfefferle, G.L. Haller, J. Catal. 253 (2008) 74–90.
[30] C. Hess, R. Schlögl, Chem. Phys. Lett. 432 (2006) 139–145.
[31] F. Gao, Y. Zhang, H. Wan, Y. Kong, X. Wu, L. Dong, B. Li, Y. Chen, Micropor. Mesopor. Mater. 110 (2008) 508–516.
[32] M. Baltes, K. Cassiers, P. Van Der Voort, B.M. Weckhuysen, R.A. Schoonheydt, E.F. Vansant, J. Catal. 197 (2001) 160–171.
[33] C.T. Kresge, M.E. Leonowicz, W.J. Roth, J.C. Vartuli, J.S. Beck, Nature 359 (1992) 710–712.
[34] X. Hao, Y. Zhang, J. Wang, W. Zhou, C. Zhang, S. Liu, Micropor. Mesopor. Mater. 88 (2006) 38–47.
[35] D. Zhao, Q. Huo, J. Feng, B.F. Chmelka, G.D. Stucky, J. Am. Chem. Soc. 120 (1998) 6024–6036.
[36] F. Cheng, Y.C. Lin, H.H. Cheng, Y.C. Chen, Chem. Phys. Lett. 382 (2003) 496–501.
[37] T.W. Kim, R. Ryoo, M. Kruk, K.P. Gierszal, M. Jaroniec, S. Kamiya, O. Terasaki, J. Phys. Chem. B 108 (2004) 11480–11489.
[38] P. Kuśtrowski, Y. Segura, L. Chmielarz, J. Surman, R. Dziembaj, P. Cool, E.F. Vansant, Catal. Today 114 (2006) 307–313.
[39] B.S. Liu, G. Rui, R.Z. Chang, C.T. Au, Appl. Catal. A: Gen. 335 (2008) 88–94.
[40] H. Chu, L. Yang, Q. Zhang, Y. Wang, J. Catal. 241 (2006) 225–228.
[41] T. Tsoncheva, M. Linden, S. Areva, Ch. Minchev, Catal. Commun. 7 (2006) 357–361.
[42] T. Klimovaa, L. Lizamaa, J.C. Amezcuaa, P. Roqueroa, E. Terrés, J. Navarreteb, J.M. Domínguez, Catal. Today 98 (2004) 141–150.
[43] Y. Zhu, Y. Dong, L. Zhao, F. Yuan, H. Fu, Chin. J. Catal. 29 (2008) 1067–1069.
[44] B.R. Jermy, S.Y. Kim, K.V. Bineesh, M. Selvaraj, D.W. Park, Micropor. Mesopor. Mater. 121 (2009) 103–113.
[45] J.C. Amezcua, L. Lizama, C. Salcedo, I. Puente, J.M. Domínguez, T. Klimova, Catal. Today 107–108 (2005) 578–588.
[46] B.R. Jermy, S.Y. Kim, K.V. Bineesh, D.W. Park, Micropor. Mesopor. Mater. 117 (2009) 661–669.
[47] A. Bordoloi, A.P. Amrute, S.B. Halligudi, Catal. Commun. 10 (2008) 45–48.
[48] C.M. Yang, H.S. Sheu, K.J. Chao, Adv. Funct. Mater. 12 (2002) 143–148.
[49] C. Yang, P. Liu, Y. Ho, C. Chiu, K. Chao, Chem. Mater. 15 (2003) 275–280.
[50] H.X. Jin, Q.Y. Wu, C. Che, D.L. Zhang, W.Q. Pang, Micropor. Mesopor. Mater. 97 (2006) 141–144.
[51] F. Klose, T. Wolff, H. Lorenz, A.S. Morgenstern, Y. Suchorski, M. Piórkowska, H. Weiss, J. Catal. 247 (2007) 176–193.
[52] C. Lee, T. Lin, C. Mou, J. Phys. Chem. C 111 (2007) 3873–3882.